Remote Sensing of Environment 113 (2009) 1462–1472

Contents lists available at ScienceDirect

Remote Sensing of Environment

journal homepage: www.elsevier.com/locate/rse

Remote monitoring of tamarisk defoliation and evapotranspiration following saltcedar leaf beetle attack

Philip E. Dennison [a,*], Pamela L. Nagler [b], Kevin R. Hultine [c], Edward P. Glenn [d], James R. Ehleringer [c]

[a] Center for Natural and Technological Hazards and Department of Geography, University of Utah, Salt Lake City, UT 84112, USA
[b] United States Geological Survey, Southwest Biological Science Center, Sonoran Desert Research Station, BioSciences East Building, Tucson, AZ 85721, USA
[c] Department of Biology, University of Utah, Salt Lake City, UT 84112, USA
[d] Department of Soil, Water and Environmental Science, University of Arizona, Tucson, AZ 85721, USA

ARTICLE INFO

Article history:
Received 21 December 2007
Received in revised form 1 April 2008
Accepted 24 May 2008

Keywords:
Insect defoliation
Change detection
MODIS
ASTER
Evapotranspiration
Colorado Plateau

ABSTRACT

Tamarisk (*Tamarix* spp.) has invaded riparian ecosystems throughout the Western United States, including significant portions of riparian ecosystems within U.S. National Parks and Monuments. Recently, the saltcedar leaf beetle (*Diorhabda elongata*) was released as a tamarisk biocontrol agent. Although initial releases have been monitored, no comprehensive program is currently in place to monitor the rapid spread of *Diorhabda* that has resulted from numerous subsequent releases by county and state agencies. Long term monitoring of tamarisk defoliation and its impacts on habitat and water resources is needed. This study examines the potential for using higher spatial resolution Advanced Spaceborne Thermal Emission and Reflection Radiometer (ASTER) data and lower spatial resolution Moderate Resolution Imaging Spectroradiometer (MODIS) data for monitoring defoliation caused by *Diorhabda* and subsequent changes in evapotranspiration (ET). Widespread tamarisk defoliation was observed in an eastern Utah study area during summer 2007. ASTER normalized difference vegetation index (NDVI) showed only minor changes between 2005 and 2006, but a significant drop in NDVI was found within riparian areas between 2006 and 2007. The decrease in NDVI caused by defoliation was apparent despite partial refoliation within the study area. MODIS time series data revealed that absolute decline in EVI varied by site, but that the timing of EVI decline during summer 2007 was early with respect to phenological patterns from 2001 through 2006. Defoliation caused decreases in ET values estimated from both ASTER and MODIS data. MODIS estimated ET declined earlier than in previous years, although annual ET was not significantly different than ET in previous years due to high year-to-year variability. Challenges to detection and monitoring of tamarisk defoliation include spectral mixing of tamarisk and other cover types at subpixel spatial resolution, spatial coregistration of time series images, the timing of image acquisition, and changes unrelated to defoliation in non-tamarisk land cover over time. Continued development of the techniques presented in this paper may allow monitoring the spread of *Diorhabda* and assessment of potential water salvage resulting from biocontrol of tamarisk.

© 2009 Elsevier Inc. All rights reserved.

1. Introduction

1.1. "The tamarisk problem"

Tamarisk (*Tamarix* spp.) was introduced to the United States from Asia more than a century ago for soil erosion control and landscaping purposes. Since its introduction to the western United States, tamarisk has become dominant or sub-dominant over many arid and semi-arid river systems. Its current spread throughout arid riparian corridors is at rates exceeding 20 km per year (Busch & Smith, 1995; DiTomosa, 1998; Glenn & Nagler, 2005; Smith et al., 1998; Zavaleta, 2000). The presence of tamarisk in western North America has been cited for reducing water availability for human enterprise, reducing biodiversity, displacing native vegetation (particularly cottonwood and willow tree species) and for reducing habitat quality for wildlife (Bailey et al., 2001; DiTomosa, 1998; Glenn & Nagler, 2005; Johnson, 1987; Rice et al., 1980; Stromberg, 1998). Tamarisk has successfully replaced much of the native riparian vegetation in some of the most valued protected lands in the southwestern United States, including national park lands. In doing so, tamarisk has had a significant impact on recreation, wildlife and ecosystem services of the park system (Zavaleta, 2000). National Parks that include river systems sufficiently large for boating activities have experienced declines of instream use associated with tamarisk invasion. For instance, in the Grand Canyon alone, transpiration by tamarisk decreases the period of optimal boating flows to the extent that the estimated economic loss is over $2,000,000 per year (Penny, 1991). The total annual losses in economic services caused by tamarisk in 1998 have been estimated as between 133 and 285 million U.S. dollars (Zavaleta, 2000). However, more recent reviews

* Corresponding author.
E-mail address: dennison@geog.utah.edu (P.E. Dennison).

0034-4257/$ – see front matter © 2009 Elsevier Inc. All rights reserved.
doi:10.1016/j.rse.2008.05.022

have shown that tamarisk can have positive environmental impacts in riparian ecosystems (Glenn & Nagler, 2005), and that water use might be much lower than was previously assumed (Nagler et al., 2005a; Owens & Moore, 2007).

1.2. Study rationale

Tamarisk control has become an important aspect of local, state, and federal government efforts to manage public and private lands. Costly eradication and restoration efforts are currently ongoing along many riparian corridors, but attempts to eradicate tamarisk have been met with variable success. Traditional control strategies such as mechanical removal, fire, and herbicidal treatments have proven costly, unsuccessful, or have had unintended negative ecological impacts. An alternative biological control program was developed to control the spread of tamarisk. In 1996, the United States Department of Agriculture (USDA) Animal and Plant Health Inspection Service (APHIS) approved the saltcedar leaf beetle (*Diorhabda elongata* Brulle) from central Asia for use as a tamarisk biocontrol agent (DeLoach et al., 2000; Dudley, 2005).

Diorhabda has been released in multiple locations across the Western U.S. with varying results (Dudley et al., 2001; Dudley, 2005). Ground-based monitoring of beetle expansion is difficult and therefore it is not clear what impact the beetle is having over large spatial scales. For example, on the Colorado Plateau where the beetle has been released at several locations, there are currently no comprehensive programs in place to track the movement of the beetle and subsequent defoliation of tamarisk. Moreover, there are no programs in place to monitor defoliation impacts on water resources, recreation, riparian habitat, or endangered species within the Colorado Plateau region.

Remotely sensed data offer a potential means for monitoring tamarisk defoliation and changes in evapotranspiration (ET) caused by defoliation, but the temporal and spatial resolutions of existing remotely sensed data may not be well-suited for this task. Temporal resolution on the order of days to weeks is needed for monitoring rapid defoliation by *Diorhabda* and subsequent changes in ET. Sensors capable of imaging with this frequency, such as the Moderate Resolution Imaging Spectroradiometer (MODIS), have a relatively low spatial resolution (250–500 m) that cannot resolve small tamarisk stands. Higher spatial resolution data, such as 15 m spatial resolution data from the Advanced Spaceborne Thermal Emission and Reflection Radiometer (ASTER), may be capable of mapping defoliated areas, but can only do so infrequently.

This research assesses the abilities of data from a higher spatial resolution, infrequently available sensor (ASTER) and from a lower spatial resolution, more frequently available sensor (MODIS) to detect and monitor tamarisk defoliation and resulting changes in ET. Our goal is to develop and test remote sensing techniques that will allow quantitative assessment of *Diorhabda*'s impact on tamarisk phenology and water use on the Colorado Plateau across large spatial and temporal scales.

2. Background

2.1. Diorhabda elongata

Diorhabda is promoted as a biocontrol agent for tamarisk because it feeds selectively on tamarisk foliage in the larval and adult stages. Pupation and adult over-wintering take place in the litter beneath tamarisk. The beetle emerges from dormancy several weeks after tamarisk flushes new foliage in the spring, and beetles immediately begin foraging on tamarisk leaves. In theory, repeated defoliation by the beetle should progressively reduce carbohydrate reserves of individual shrubs and ultimately result in widespread mortality.

Results from previous releases of *Diorhabda* have been mixed. In northern Nevada, *Diorhabda* defoliated 20,000 ha of tamarisk within three years of its initial release along the lower Humboldt River (Dudley, 2005). However, nearly all the defoliated tamarisk produced new leaves within weeks after complete defoliation. Nevertheless, tamarisk live tissue volume decreased after each subsequent defoliation event, resulting in reduced evapotranspiration, greater wildlife use, and increased biodiversity (Dudley, 2005). Other releases in Wyoming, Colorado, and California have been met with only moderate success, and no releases have been successful south of 38° N. Reproduction by the beetle requires a minimum day length of 14.5 h (Dudley, 2005). Therefore at latitudes below approximately 38° N, reproduction does not occur, or only occurs during a very short period. Other geographic biotypes of *Diorhabda* from lower latitudes are currently being considered for future releases (Dudley, 2005).

In the summer of 2004 through the summer of 2006, *Diorhabda* was released at multiple locations along the Colorado River, near Moab, Utah. The goal of the beetle releases was to facilitate an aggressive long-term eradication and restoration program in eastern Utah. Due to the remote landscape of the Colorado Plateau, ground-based monitoring of beetle expansion is difficult. Thus, it is not currently clear what impacts the beetle is having over large spatial scales.

2.2. Remote sensing of defoliation

Defoliation of tamarisk by *Diorhabda* results in a substantial, near complete loss of leaf area. This decrease in leaf area has multiple impacts on canopy reflectance. Chlorophyll absorption decreases, which in turn increases reflectance in the visible spectral region, particularly in red wavelengths. Near infrared reflectance declines due to the loss of leaf additive reflectance. Vegetation indices can be used to measure changes in leaf area resulting from defoliation (Nelson, 1983). One simple vegetation index, the Normalized Difference Vegetation Index (NDVI; Rouse et al., 1973), is calculated as:

$$\mathrm{NDVI} = \frac{\rho_{NIR} - \rho_{red}}{\rho_{NIR} + \rho_{red}} \tag{1}$$

where ρ_{NIR} is the reflectance of the near infrared bands and ρ_{red} is the reflectance of the red band. As defoliation occurs and leaf area decreases, the NDVI value will also decrease. More complex vegetation indices correct for variations in soil background and for atmospheric scattering. The Enhanced Vegetation Index (EVI; Huete et al., 2002) is the standard vegetation index for MODIS. EVI is calculated as:

$$\mathrm{EVI} = 2.5 \times \frac{\rho_{NIR} - \rho_{red}}{\rho_{NIR} + 6 \times \rho_{red} - 7.5 \times \rho_{blue} + 1} \tag{2}$$

where ρ_{blue} is the reflectance of the blue band. Like NDVI, EVI will decrease in response to defoliation.

Previous studies have used vegetation indices or other measures to examine canopy defoliation by a variety of insects. Mapping of gypsy moth (*Lymantria dispar* L.) defoliation in the Eastern U.S. was one of the first applications developed for satellite multispectral remotely sensed data. Rohnde and Moore (1974) used multidate Landsat data to resolve confusion between gypsy moth defoliation and sparsely vegetated land cover. Nelson (1983) calculated the difference between vegetation indices on two Landsat dates, and then empirically determined a threshold to separate defoliated from non-defoliated pixels. This technique was found to be superior to competing techniques for the most accurate assessment of defoliated area. Joria et al. (1991) compared the abilities of Landsat Thematic Mapper and SPOT data to map gypsy moth defoliation severity classes. Landsat Enhanced Thematic Mapper+ data acquired over three years were used by Townsend et al. (2004) to map gypsy moth defoliated area to explain changes in stream nitrogen concentrations.

Multispectral remote sensing has also been used to examine canopy defoliation by other insects. Previous studies have used single date (Franklin & Raske, 1994; Leckie & Ostaff, 1988) and multidate (Franklin et al., 1995a; Radeloff et al., 1999) multispectral remotely sensed data to map budworm (*Choristoneura* spp.) defoliation. Radeloff et al. (1999) went beyond detection of defoliation to directly compare remote sensing measures to budworm population data. Multispectral remote sensing has also been used to detect defoliation caused by adelgid (*Adelges* spp.) infestations (Franklin et al., 1995b; Royle & Lathrop, 2002). Royle and Lathrop (2002) used multidate Landsat TM data to calculate changes in vegetation indices, which were then used to discriminate multiple defoliation classes. Fraser and Latifovic (2005) used 1 km spatial resolution SPOT Vegetation data to map defoliation caused by hemlock looper (*Lambdina fiscellaria*). They concluded that coarse resolution data held promise for mapping looper defoliation, although a large number of false positive detections of defoliation may limit monitoring effectiveness. Numerous studies have examined using remote sensing to detect canopy mortality caused by mountain pine beetle (*Dendroctonus ponderosae*) (Coops et al., 2006; Franklin et al., 2003; Renz & Nemeth, 1985; Sirois & Ahern, 1988; White et al., 2007; Wulder et al., 2005). Although mountain pine beetles do not feed directly on leaves or branches, their galleries may eventually girdle trees, resulting in total canopy mortality followed by defoliation.

These previous studies indicate that remote monitoring of tamarisk defoliation caused by the saltcedar leaf beetle may be feasible. However, there are important distinctions between previously studied forest-defoliation and tamarisk defoliation. In contrast to largely continuous forest canopies, tamarisk colonizes thin strips along stream banks that are often only meters to tens of meters wide. As a consequence, these tamarisk stands (and thus tamarisk defoliation) cover only a fraction of a pixel at lower spatial resolutions. Upslope of tamarisk stands, water availability is often very limited and vegetation biomass rapidly decreases. Thus, despite occupying a narrow spatial extent, tamarisk stands may still create the dominant vegetative signal within a large pixel.

2.3. Estimating tamarisk evapotranspiration from remotely sensed data

Water salvage is an important part of the rationale for controlling tamarisk, and thus a remote sensing method is needed to monitor evapotranspiration (ET) at landscape scales. Several methods have previously been used to estimate ET from satellite data. ET can be estimated using a combination of Landsat Thematic Mapper optical and thermal infrared (TIR) bands. These bands are used to solve the surface energy balance for the latent heat of evaporation in so-called "one-source" models, such as the Mapping Evapotranspiration with Internalized Calibration (Allen et al., 2007) or the Surface Energy Balance Algorithm (Bastiaanssen et al., 1998) models. In so-called "two-source" models, the landscape is divided into vegetated and non-vegetated fractions using NDVI, then sensible and latent heat fluxes are estimated separately for vegetation and soil using TIR and meteorological data (Kustas & Norman, 1999). The Triangle Method (Carlson, 2007) plots NDVI against land surface temperature (LST) derived from the TIR band to reveal LST–NDVI anomalies, a sign of plant stress. Landsat-based methods are basically snapshots of ET due to the long return time needed to acquire multiple images.

ET can also be estimated by using time series VIs from frequent-return satellite sensor systems such as MODIS, and calibrated against ground measurements of actual ET measured at flux towers (e.g., Yang et al., 2006) or potential ET determined at micrometeorological stations (e.g., Mu et al., 2007). Time series methods are useful for monitoring changes in ET over time, such as the effects of beetle damage on tamarisk in the present study, although spatial resolution is sacrificed. Nagler et al. (2005a,b) developed an algorithm for estimating ET by riparian vegetation in the southwestern U.S., including tamarisk. ET can be estimated using the equation:

$$\mathrm{ET} = 11.5 \times \left(1 - e^{-1.63 \cdot EVI^*}\right) \times \frac{0.883}{1 + e^{\frac{-(T_a - 27.9)}{2.57}}} + 1.07 \quad (3)$$

where T_a is the maximum daily air temperature with units of °C and ET has units of mm day^{-1}. The first term containing EVI* represents scaled foliage density, based on the formula for light extinction through a canopy. EVI* is calculated by scaling EVI values between 0 and 1 using minimum and maximum EVI values:

$$\mathrm{EVI}^* = 1 - (\mathrm{EVI}_{max} - \mathrm{EVI}) / (\mathrm{EVI}_{max} - \mathrm{EVI}_{min}) \quad (4)$$

Nagler et al. (2005a) established EVI_{min} and EVI_{max} coefficients of 0.091 and 0.542, respectively, based on the maximum and minimum EVI values found at nine tower sites over a period of four years.

The second term containing T_a correlates with the atmospheric water demand, an advective term in the Penman–Monteith equation (Monteith & Unsworth, 1990). The temperature term is in the form of a sigmoidal curve, where there is a minimum T_a (20 °C), below which stomatal conductance approaches maximum; a middle, exponential portion of the curve which fits the vapor pressure deficit:temperature response in the Penman–Monteith equation; and an upper limit (35 °C), where stomatal conductance approaches zero and plant transpiration is

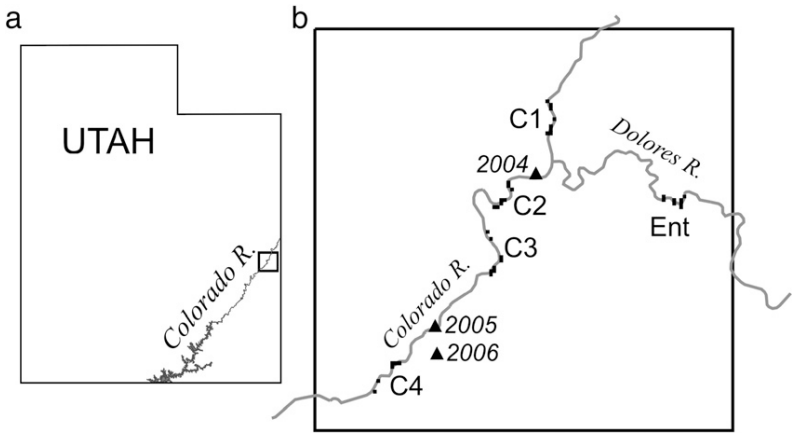

Fig. 1. a) The location of the 23 km by 23 km study area in eastern Utah. b) Five sites in relation to the bounding box of the study area: Ent (Entrada) along the Dolores River, and 4 sites along the Colorado River (C1, C2, C3, and C4). Small black squares indicate the locations of the 6–8 MODIS pixels extracted for each site. Black triangles indicate the approximate locations of saltcedar leaf beetle releases, accompanied by the year of release in italics.

constrained. When the EVI* term in Eq. (3) goes to zero (no foliage), the projected ET is simply equal to the minimum value given by the constant 1.07 mm day^{-1}, consistent with ET rates in riparian areas during the dormant season. This minimum value is within the range of minimum values measured at flux towers in riparian corridors. ET does not increase with temperature without foliage present, so at any given temperature, ET will be proportional to EVI*.

Calibration done by Nagler et al. (2005a) found that Eq. (3) had a root mean square error of 1.09 mm day^{-1}, or about 25% of the mean ET value across multiple tower sites. At the three tower sites dominated by tamarisk (two on the Middle Rio Grande and one on the Lower Colorado River), predicted ET (3.7 mm day^{-1}) was nearly identical to measured ET (3.8 mm day^{-1}) over multiple years of measurement. This algorithm for estimating ET has been validated in subsequent studies in western riparian zones (Nagler et al., 2007a; Scott et al., 2008), and the general approach of estimating ET from MODIS vegetation indices and ground data has been applied to other ecosystems, including semi-arid grasslands and shrublands (Nagler et al., 2007b), and at regional (e.g., Cleugh et al., 2007) and continental (e.g., Mu et al., 2007; Yang et al., 2006) measurement scales.

3. Methods

3.1. Study area

The potential for remote monitoring of tamarisk defoliation by saltcedar leaf beetles was investigated within a 23 km by 23 km area of eastern Utah (Fig. 1). The Colorado River flows through the study area from northeast to southwest. A major tributary, the Dolores River, flows west from Colorado and intersects the Colorado River near Dewey Bridge, Utah. Dominant native riparian tree species within the study area include Fremont cottonwood (*Populus fremontii* Wats.) and multiple willow species (*Salix* spp.). Tamarisk (*Tamarix ramosissima* Ledeb) has extensively colonized stream banks throughout the study area, forming dense stands that reach up to 200 m from the rivers' edges.

Diorhabda was released in three different locations within the study area, indicated in Fig. 1 (Tim Higgs, pers. comm.). The first release took place on August 18, 2004 near the confluence of the Dolores and Colorado Rivers. Subsequent releases downstream from the initial release site took place on July 28, 2005 and July 14, 2006. It is not clear which release or releases caused widespread defoliation by *Diorhabda* throughout the entire study area during the summer of 2007. Defoliation also occurred within a small portion of the study area near the confluence of the Dolores and Colorado Rivers by fall 2006 (Dan Bean, pers. comm.).

Five sites within the study area were selected for field and remote sensing analysis. The primary site was located along the Dolores River at the University of Utah Entrada Field Station (Fig. 1). Sap flux measurements at this location were collected from June 17 through leaf senescence in early November, 2007 in association with a long-term monitoring effort taking place at this site. Polygons dominated by tamarisk were recorded at the Entrada site and at four secondary sites along the Colorado River. The Colorado River secondary sites were numbered 1 through 4 from north to south (Fig. 1).

3.2. Sap flux measurements

Granier-type temperature sensors (Granier 1987, 1996; Hultine et al., 2007) were constructed to measure sap flux density (J_s, g H_2O m^{-2} sapwood s^{-1}). Each sensor consisted of a pair of 10 mm long, 2 mm diameter stainless steel probes inserted approximately 15 cm apart along the axis of the hydroactive xylem (i.e. sapwood). The azimuth direction of each sensor was randomly selected to eliminate potential biases due to non-uniformity in sap flux around the stem. The upper probe (i.e. toward the canopy) was supplied with constant heat of 200 mW, and the temperature difference between the heated probe and the lower, unheated reference probe was converted to sap flux density according to Granier (1987, 1996):

$$J_s = 0.0119 \left(\frac{\Delta T_0}{\Delta T} - 1\right)^{1.23} \quad (5)$$

where ΔT is the temperature difference between the heated and unheated probes and ΔT_0 is the temperature difference obtained under zero flow conditions. We assumed that zero flow only occurred at night when vapor pressure deficit was at or near zero.

Nineteen tamarisk trees were selected for study with stem diameters ranging from 7.5 to 13.8 cm with a mean diameter of 10.0 cm. Each tree was dominant or sub-dominant and received sunlight throughout daylight hours. A single sensor was inserted into the main stem of each tree at approximately 1.5 m above the ground. Temperature differences of all sensors were logged every 30 s and stored as 30 min averages with Campbell CR10X-2M data loggers (Campbell Scientific, Logan, UT, USA). Because sap flux studies on these trees are ongoing, we have not yet determined sapwood area/ground area, or leaf area/sapwood area relationships in order to scale sap flux density to stand transpiration. Therefore J_s was not scaled to compare with ET estimated from remotely sensed data, but was instead used to reveal water use patterns in response to defoliation.

3.3. Tamarisk polygons

To spatially isolate changes in remote sensing vegetation indices caused by tamarisk defoliation, polygons dominated by tamarisk were mapped at each of the five field sites. One-meter spatial resolution false-color digital orthophotographs acquired in 2006 by the USDA National Agriculture Imagery Program (NAIP) were used to create initial polygons. Brightness and texture were used to find areas at least 30 m by 30 m (0.09 ha) in extent with homogeneous canopy characteristics. Polygons were digitally outlined and then visited in early October 2007. Canopy dominance was visually estimated, and validated polygons were required to have at least 90% tamarisk canopy dominance. Evidence of defoliation was noted at all polygons in the study area, although new tamarisk leaf growth had apparently occurred in many of the polygons. A total of 56 polygons were field validated for use in the remote sensing analysis. The smallest polygon had an area of 0.13 ha, and the largest polygon had an area of 1.04 ha. The mean polygon area was 0.41 ha.

3.4. ASTER data

ASTER is a multispectral sensor with instruments covering three different spectral ranges. A 15-m spatial resolution visible/near infrared (VNIR) sensor has 3 bands that cover green, red, and near infrared wavelengths. A 30-m spatial resolution sensor has 6 bands that cover shortwave infrared wavelengths. The third sensor covers the thermal infrared with 5 bands at a 90-m spatial resolution. Given the narrow width of tamarisk stands within the study area, only data from the VNIR sensor with 15-m spatial resolution were used for this study.

ASTER scenes containing the study area were acquired in 2005, 2006, and 2007. The first ASTER scene was acquired on September 1, 2005. Scattered clouds within the study area obscured portions of the Colorado and Dolores Rivers, but clouds and their shadows did not cover any of the validated polygons. The 2006 ASTER scene was acquired on July 18, before the apparent start of widespread *Diorhabda* activity within the study area. The 2007 ASTER scene was acquired on September 7, after tamarisk defoliation occurred throughout the entire study area during the 2007 growing season. All three scenes were ordered from the NASA Land Processes Distributed Active Archive Center (LPDAAC) as level 3 orthorectified calibrated radiance images (AST14OTH). All three ASTER calibrated radiance images were processed

Table 1
Image coregistration statistics within the study area for the three ASTER images.

Image comparison	# of tie points	Maximum single point RMSE (pixels)	Mean single point RMSE (pixels)	Total RMSE (pixels)
2005–2006	87	1.35	0.46	0.56
2006–2007	90	1.22	0.31	0.46
2005–2007	84	1.44	0.44	0.54

to apparent surface reflectance using Atmospheric CORrection Now (ACORN version 5, ImSpec LLC).

ASTER image coregistration was assessed using the ENVI (version 4.3, ITT Visual Information Solutions) automatic image registration tool. This tool finds areas with similar single band reflectance patterns between two images and assigns tie points. The root mean square error (RMSE) of the tie points, based on an assumed first degree polynomial transformation, is a measure of the coregistration error between the two images. Up to 100 tie points were automatically selected for the near infrared band, and points obviously impacted by cloud cover or shadows were manually discarded. Maximum, mean, and total RMSE values within the study area are shown in Table 1.

NDVI was calculated from the apparent surface reflectance images and NDVI values were extracted for all pixels that were more than 50% within a validated polygon. Approximately 1100 NDVI values were extracted from each of the 2005, 2006, and 2007 images. Histograms were used to examine the distribution of tamarisk NDVI values on each date. Changes in NDVI between 2005 and 2006, and between 2006 and 2007, were calculated for each extracted pixel. Histograms were also used to examine changes in the distribution of tamarisk NDVI changes between each date. Based on classification rules empirically derived from the NDVI and NDVI change distributions, defoliated tamarisk stands were classified from the 2007 NDVI image. These classification rules are described in the Results section.

3.5. MODIS data

There are two major considerations for using MODIS data to monitor tamarisk defoliation: spatial resolution and temporal resolution. At a nominal spatial resolution of 250 m for the red and near infrared bands, tamarisk stands within the study area cover a minority of any MODIS pixel. The maximum coverage of the tamarisk polygons within any 250 m MODIS product pixel was 29%, and the minimum coverage was 3%. The mean polygon coverage within 38 MODIS pixels used to measure vegetation index response to defoliation was 11%.

Since tamarisk stands are such a small areal fraction of 250 m MODIS pixels, vegetation index response to defoliation will be damped by non-tamarisk contributions to pixel reflectance. The small areal coverage of tamarisk stands can be made worse by view zenith angle effects. MODIS has a 16-day repeat cycle, and for each day of the cycle the observational area of each pixel will be different. As view zenith angle increases, the effective observational area of each MODIS pixel also increases (e.g. Wolfe et al., 1998). While MODIS red and near infrared bands may have a nominal spatial resolution of 250 m, the actual spatial resolution on days with high view zenith angles may be much lower. Lower effective spatial resolution can thus further dampen vegetation index response to defoliation.

The second major consideration for using MODIS data to detect the timing of defoliation is temporal resolution. MODIS data are acquired daily within the study area, but using a daily MODIS product for monitoring defoliation is impractical for several reasons. Cloud cover can frequently obscure the sensor's view of the surface, and partial cloud cover or cloud shadows can decrease the quality of the MODIS vegetation index products. Changing view zenith and azimuth angles throughout the 16-day repeat cycle can also impact vegetation index quality. Vegetation reflectance is more strongly directional in visible wavelengths than in the near infrared, so vegetation indices vary with view zenith (Holben & Fraser, 1984). Changes in effective pixel observational area will cause further fluctuation in vegetation index values.

Temporal compositing can be used to reduce the impacts of cloud artifacts and view zenith angle (Dennison et al., 2007; Holben, 1986; Qi & Kerr, 1997). A temporal compositing algorithm selects a spectrum or index from a single date within a range of dates for each pixel. While decreasing variability and thus increasing the quality of a time series, compositing greatly reduces the temporal resolution of the time series. Two composited, 250 m MODIS vegetation index products are available from the LPDAAC: a 16-day composite and a monthly composite. We selected the Terra 250 m 16-day vegetation indices product (MOD13Q1), containing NDVI and EVI, for evaluation of the defoliation monitoring abilities of MODIS.

The 16-day vegetation index product was obtained from LPDAAC for the period of March 2000 through November 2007. All of the MODIS data were reprojected from sinusoidal to Universal Transverse Mercator projection (UTM) to match the projection of the NAIP, polygon, and ASTER data. Between 6 and 8 pixels containing validated polygons were selected for each of the five sites along the Colorado and Dolores Rivers. The locations of these pixels are indicated by the black squares in Fig. 1. NDVI and EVI values were extracted for each of these pixels. Each index exhibited an annual phenological cycle characteristic of deciduous species, increasing with leaf-out in the spring and decreasing with leaf drop in the fall. EVI was selected for further evaluation due to its lower variability, especially in summer months, relative to NDVI; and due to recent use of EVI for change detection (e.g. Mildrexler et al., 2007).

Defoliation produces a decrease in EVI that is similar in magnitude to the normal phenologically-driven decrease that occurs in mid-October through mid-November. The 2000–2007 MODIS time series was analyzed to determine whether the 2007 decrease in EVI occurred anomalously early. EVI values were extracted from 6–8 pixels containing tamarisk polygons for each of the five sites (Fig. 1). To reduce the impact of spatial variability in tamarisk cover, the mean EVI for each site was calculated for each composite period. For each year in the time series, the steepest decline over two compositing periods was calculated using the average EVI values for each site:

$$\Delta EVI = EVI_i - EVI_{i+2} \quad (6)$$

where i is the composite number. The time span of two consecutive compositing periods was selected to detect sustained declines in EVI. Single compositing periods often had declines in EVI that were not linked to phenology or defoliation, but were likely caused by changes in view zenith angle. The steepest decline in EVI (ΔEVI_{min}) was

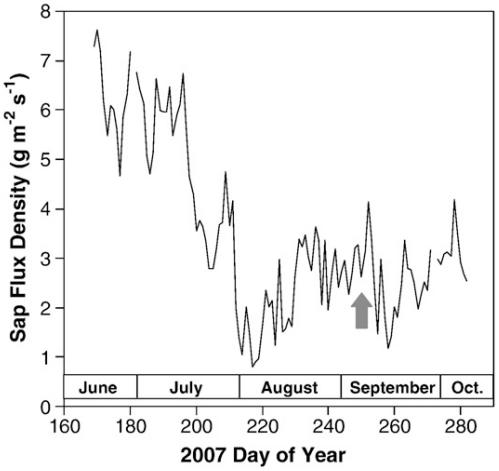

Fig. 2. Daily sap flux density measured at the Entrada site. The arrow indicates the date of the 2007 ASTER acquisition.

determined by finding the minimum ΔEVI value. The central date of ΔEVI_{min} was calculated by averaging the first day of the composite period i and the last day of the composite period $i+2$. Comparison of EVI trends at the five sites demonstrated that the sites differed in their magnitude of EVI change in response to defoliation.

3.6. Estimation of evapotranspiration

The algorithm developed by Nagler et al. (2005a) was used to estimate ET at the Entrada site from both MODIS and ASTER data. MODIS ET was estimated for 16-day intervals corresponding to MODIS composites acquired between March 1 and November 1. This time period contains the growing season in eastern Utah. EVI values were converted to scaled EVI (EVI*) using EVI_{min} and EVI_{max} scaling coefficients from Nagler et al. (2005a). EVI* values were calculated for the eight MODIS pixels selected for the Entrada site, including the single pixel that contained the sap flux measurement site.

ET was also estimated from the ASTER data. Approximately 240 15-m ASTER pixels corresponding to the area of each 250-m MODIS pixel were extracted. Since ASTER does not have the blue band necessary for calculating EVI, a second order polynomial relationship between ASTER NDVI and MODIS EVI* were derived and used to transform ASTER NDVI to EVI* (Nagler et al., 2007b). For both the MODIS and ASTER ET estimations, maximum daily air temperature (T_a) was calculated from data recorded at a weather station in Moab (University of Oregon, Solar Radiation Monitoring Lab, http://solardat.uoregon.edu/Moab.html). This station is located approximately 38 km from the Entrada site and 270 m lower in elevation.

ET estimates are simply transformations of vegetation index values, allowing foliage density to be expressed in units of plant water consumption as determined by relationships between moisture flux tower results and EVI values (Nagler et al., 2005a, 2007a; Scott et al., 2008). For river systems examined by these previous studies and this study, the surface soil is normally dry and the vegetation is phreatophytic,

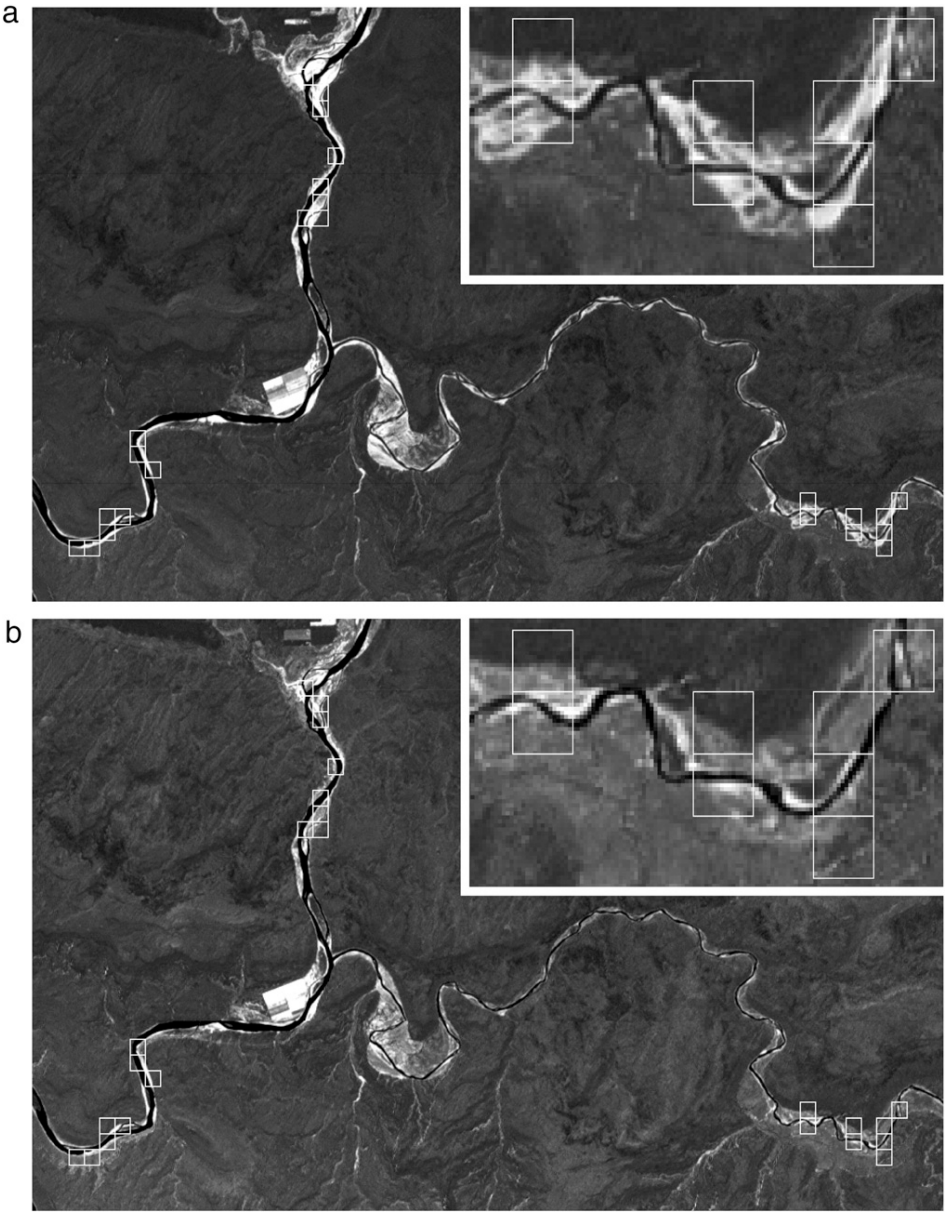

Fig. 3. a) July 18, 2006 NDVI calculated from ASTER apparent surface reflectance. NDVI is linearly scaled between 0 (black) and 0.6 (white). White outlined boxes indicate the 250-m MODIS pixels used for analysis at the Entrada (right), C1 (top) and C2 (left) sites. The inset at upper right shows the Entrada site, with the MODIS pixels covering the site outlined in white. b) September 7, 2007 NDVI for the same area, with the same scaling of NDVI. The inset at upper right shows the Entrada site.

using water from the aquifer. Hence, the bare soil evaporation component of ET was assumed to be low compared to water lost through plant transpiration. The constant term in Eq. (3), 1.07 mm day^{-1}, is an estimate of mean bare soil evaporation over an annual cycle. Given the narrow width of tamarisk stands, all MODIS pixels and some ASTER pixels will contain mixtures of tamarisk, other riparian vegetation, non-riparian vegetation, and bare soil. Other riparian vegetation should possess similar ET before and after tamarisk defoliation, and xerophytic non-riparian vegetation (dominantly greasewood (*Sarcobatus vermiculatus*) surrounding the Entrada site) will have very low ET during the summer months relative to riparian vegetation. While the presence of other riparian vegetation, non-riparian vegetation, and bare soil within pixels may increase the uncertainty in absolute values of estimated ET, estimated ET should still provide valid estimate of the decrease in ET resulting from defoliation.

Pre- and post-defoliation ET estimates were compared for both the ASTER and MODIS data. We assumed that the leaves remaining on the tamarisk plant after partial defoliation or refoliation are functionally equivalent to leaves on non-defoliated plants. These assumptions are currently under investigation at the Entrada site using the sap flux density measurements. ET estimated from the MODIS time series data for the pixel containing the sap flux site was also compared to sap flux measurements.

Changes in estimated ET were compared to the tamarisk area within MODIS pixels at the Entrada site. Tamarisk area was estimated using a point intercept visual interpretation method (Nagler et al., 2005c). A grid containing 232–266 intersections was overlaid onto a 250 m by 250 m area extracted from the NAIP image for each MODIS pixel. Vegetation type (tamarisk or non-tamarisk) or other land cover type (e.g. river, soil) was recorded at each grid intersection. Percentage tamarisk cover was calculated by dividing the number of intersections identified as tamarisk by the total number of intersections.

4. Results

4.1. Sap flux

Daily sap flux density measurements showed a rapid decline in transpiration that occurred during the last half of July 2007 (Fig. 2). Sap flux density fluctuated between 4.7 and 7.6 g m^{-2} s^{-1} between the start of measurements and day 196. After day 196, sap flux density dropped by more than 5 g m^{-2} s^{-1} over a period of 21 days. An initial drop of 4 g m^{-2} s^{-1} occurred between days 196 and 204, followed by a small recovery from days 205 through 209. The range of this recovery (approximately 2 g m^{-2} s^{-1}) is within the range of variation seen both before and after the defoliation event, so it may not represent an actual change in leaf area. The minimum sap flux density of 0.79 g m^{-2} s^{-1} was measured on day 217 (August 5). After this minimum was reached, transpiration slowly increased and then leveled off through the end of the of the measurement period. This may be due to partial refoliation that occurred at the site. However, because of background thermal gradients between the heated and unheated temperature probes, it is unclear whether the Granier-type sensors can accurately detect low flux rates such as those that occurred after initial defoliation. ASTER data were acquired during the partial refoliation period (Fig. 2). Sap flux density on the date of ASTER acquisition was 2.6 g m^{-2} s^{-1}.

4.2. ASTER

A qualitative comparison of NDVI calculated from the 2006 and 2007 ASTER images reveals subtle changes in riparian vegetation (Fig. 3). Narrow strips of vegetation with high NDVI values in the 2006 image have lower NDVI values in the 2007 image. These changes are most apparent in the magnified subset containing the Entrada Ranch site. The narrow strips with reduced NDVI closely corresponded to the areas within validated polygons at each of the five sites. Since the visual changes between ASTER images were often subtle, quantitative analysis was needed to determine the extent of change in vegetation cover caused by defoliation.

NDVI extracted from the validated polygon pixels revealed changes in the distribution of NDVI values from 2005 and 2006 to 2007 (Fig. 4a). In both 2005 and 2006, tamarisk NDVI frequency peaked at a value just below 0.6. In 2007, the peak NDVI frequency was much lower, at 0.3. In 2005, only 6.4% of the pixels within the validated polygons had an NDVI below 0.4. 2006 was similar, with 8.5% of pixels with an NDVI below 0.4. In 2007, the percentage of pixels below an NDVI of 0.4 rose to 57.9%. The Mann–Whitney *U* test was used to assess whether the distributions of NDVI values shown in Fig. 4a are significantly different (Mann & Whitney, 1947). The NDVI distributions for 2005 and 2006 were not found to be significantly different ($P=0.53$), but the distribution for 2007 was significantly different from both 2005 and 2006 ($P<0.0001$). Histograms of NDVI change demonstrate that defoliation resulted in a large drop in NDVI between 2006 and 2007 (Fig. 4b). NDVI did change between the 2005 and 2006 ASTER images, but 69.9% of pixels changed less than 0.1 in the positive or negative directions. The distribution of NDVI changes between 2005 and 2006 peaked at 0 (no change). In contrast, the peak distribution of NDVI changes decreased by 0.25 between 2006 and 2007. Only 9.7% of polygon pixels increased in NDVI between 2006 and 2007.

The distributions in Fig. 4 were used to empirically determine thresholds to be used for mapping defoliation within the study area. A decrease in NDVI in excess of 0.1 was chosen as a threshold indicator of defoliation. Only 15% of the polygon pixels decreased in excess of this threshold between 2005 and 2006, but 71% of the polygon pixels

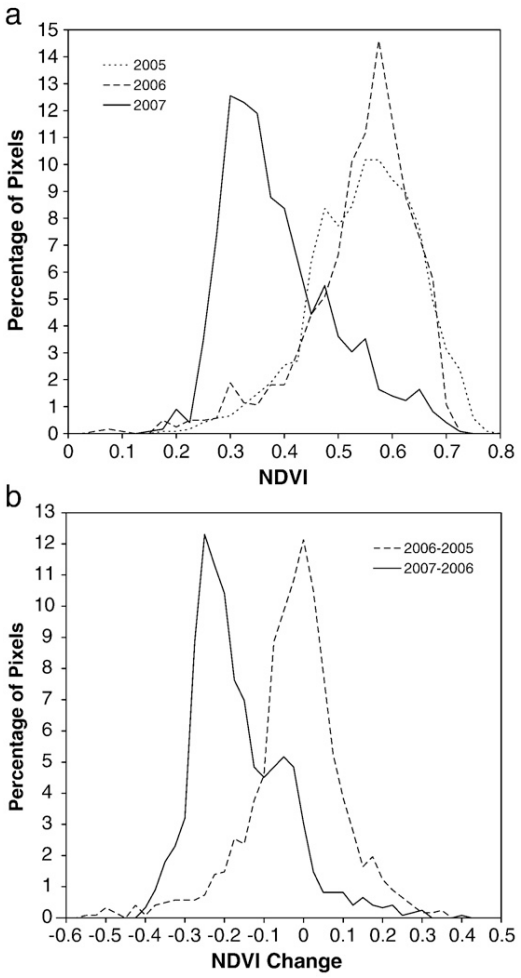

Fig. 4. a) Histograms of NDVI values for all pixels within the tamarisk polygons, extracted from the 2005, 2006, and 2007 ASTER images. b) Histograms of change in NDVI between two ASTER image dates. A negative change indicates a drop in NDVI between the earlier and later image.

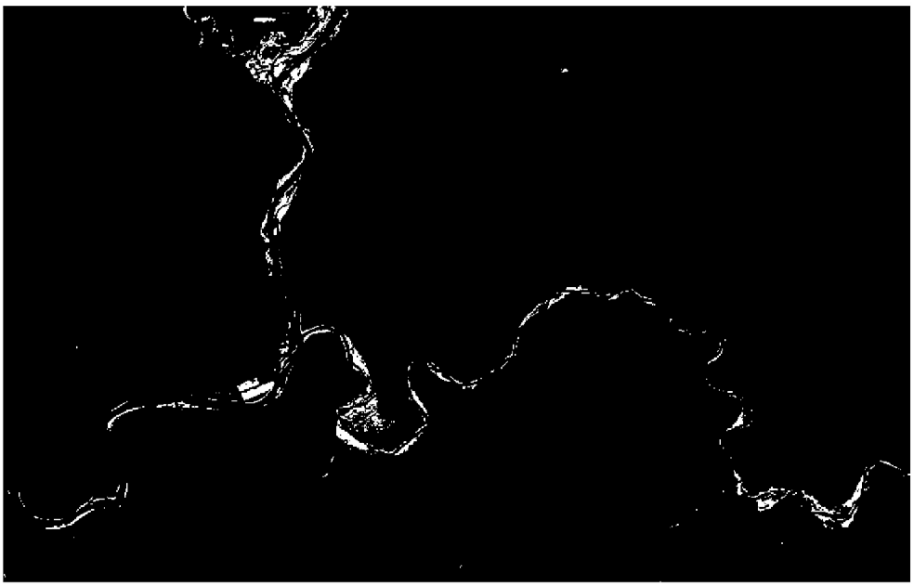

Fig. 5. Defoliated areas in the 2007 ASTER image (white) were calculated as pixels with a 0.1 or greater decrease in NDVI and a 2006 NDVI of at least 0.3. The area shown corresponds to the same area in Fig. 3.

decreased by at least this amount between 2006 and 2007. To ensure that large changes in NDVI in non-vegetated areas were not classified as defoliated, the 2006 (pre-defoliation) NDVI of classified pixels was required to be higher than 0.3. This rule was based on the observation that only 2.6% of the polygon pixels had NDVI values below 0.3 in 2006.

Defoliation was detected over approximately 0.5% of the study area, equivalent to an area of 251 ha (Fig. 5). Forty-nine of the 56 polygons had at least one pixel classified as defoliated, and half or more of the pixels were classified as defoliated in 41 polygons. The same defoliation detection method was used to classify defoliation in 2006. Small numbers of pixels were commonly classified as defoliated in many polygons, with 41 out of 56 polygons having at least one pixel classified as defoliated. Defoliation detections seldom reached a majority of polygons in 2006, with only three polygons having more that half of their pixels marked as defoliated. Detection errors most frequently occurred at the edges of tamarisk stands. Further investigation revealed that subpixel differences in registration between the 2005 and 2006 ASTER scenes produced large enough changes in NDVI to flag edge pixels as detections. This effect may also have increased the detection of apparent defoliation in the 2007 ASTER image. Defoliation was also falsely detected on alfalfa fields adjacent to the Colorado River (Fig. 5). In these cases, changes in NDVI were caused by differences in crop status between the 2006 and 2007 ASTER images.

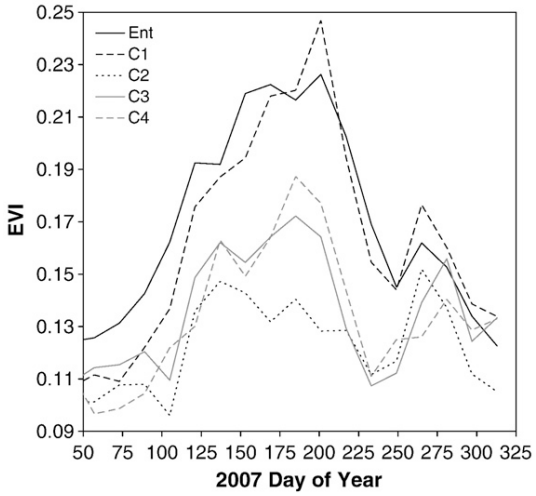

Fig. 6. Average EVI from 6–8 MODIS pixels for 5 different sites during mid-2007.

4.3. MODIS

Despite covering only a small fraction of 250-m MODIS pixels, tamarisk defoliation was apparent in the 2007 MODIS time series at four of the five sites (Fig. 6). The Entrada and C1 sites had the highest average EVI in mid-2007, and also had the most negative ΔEVI in response to defoliation. C3 and C4 displayed more moderate decreases in EVI, while C2 showed a more ambiguous, steady decline from mid-May until mid-August (Fig. 6). The magnitude of the decline in EVI in response to defoliation was proportional to the maximum EVI value for each site, indicating that percentage tamarisk cover may limit defoliation detectability in MODIS data. All sites reached a local minimum EVI between mid-August and early September. After reaching this local minimum, all sites rebounded slightly but did not approach their previous EVI maxima. The EVI minimum at the Entrada site lags the minimum sap flux density in time (Fig. 2). Minimum sap flux density occurred on August 5, while the central date of the minimum average EVI composite was September 6.

Table 2 compares the timing of ΔEVI_{min} across the entire MODIS time series for each of the five sites. From 2000–2005, ΔEVI_{min} was most often centered on day 281 or 297, corresponding with typical tamarisk senescence during the month of October. In a few cases, ΔEVI_{min} did occur earlier in the year. In 2000, a steep decline in EVI occurred in mid-to-late July at the C4 site. Since this unusually early decline predates the

Table 2
The central day of year for the largest negative change in site average EVI over two 16-day compositing periods (ΔEVI_{min}).

Year	Entrada	C1	C2	C3	C4
2000	297	297	297	297	201
2001	281	297	297	297	297
2002	297	281	281	281	281
2003	297	297	297	297	297
2004	281	265	281	329	281
2005	297	297	345	329	297
2006	297	281	233	233	281
2007	233	217	281	217	217

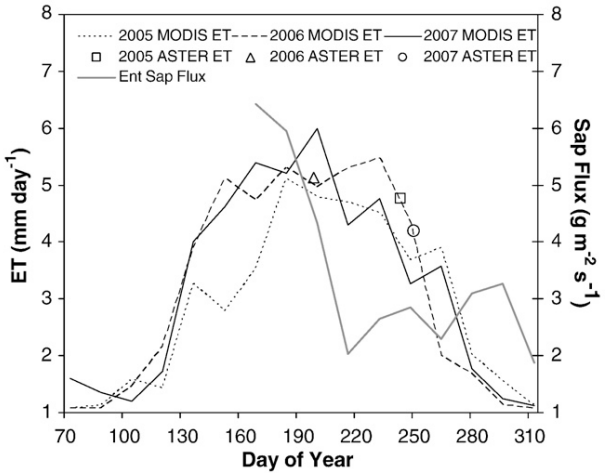

Fig. 7. 2005–2007 MODIS estimated ET and ASTER estimated ET for the MODIS pixel containing the sap flux site. The Entrada sap flux density measurements are shown for comparison.

release of *Diorhabda*, mechanical treatment of tamarisk or clearing of other vegetation at this site may have occurred at this time. Besides this one event, the earliest timing of ΔEVI_{min} was centered on day 265 for the C1 site in 2004. The steepest decline in EVI occasionally occurred later in the year, with the central dates of ΔEVI_{min} falling after day 297 in 3 instances.

In 2006, the timing of ΔEVI_{min} shifted to earlier dates for the C2 and C3 sites (Table 2). For these sites, the steepest decline in EVI was centered on day 233, corresponding to August 21. The other sites exhibited normal timing, with ΔEVI_{min} being centered on day 281 or 297. Early declines in EVI at these two sites may indicate defoliation occurred in 2006. Four of the five sites show early decline in EVI relative to 2000–2005 values (Table 2). ΔEVI_{min} was centered on day 217 (August 5) for sites C1, C3, and C4. ΔEVI_{min} was centered 1 composite later on day 233 (August 21) for the Entrada site. Only C2 had normal ΔEVI_{min} timing, due to its slow decline in EVI over the summer of 2007 (Fig. 6).

4.4. Estimated evapotranspiration

Estimated ET for the MODIS pixel containing the sap flux site varied considerably from year to year, even without defoliation. Fig. 7 shows estimated ET derived from MODIS and ASTER data for the area of the sap flux site MODIS pixel. 2005 MODIS estimated ET was lower than the 2006 and 2007 MODIS estimated ET for most of the growing season. This is apparently due to late green-up of tamarisk during 2005. The 2006 and 2007 MODIS estimated ET values were similar through day 185, although estimated ET did reach a higher peak value in 2007 than in either 2005 or 2006. MODIS estimated ET declined early in 2007 after peaking on day 201. The decline was approximately one month in advance of the steep declines in the previous two years. However, the 2007 ET decline lags the decline in sap flux (Fig. 7). ET estimated from ASTER data was higher than ET estimated from MODIS data in 2005 and 2007. Discrepancies between ASTER and MODIS estimated ET may be due to the different temporal resolutions of the two datasets. In 2006, ASTER and MODIS estimated ET closely agreed.

Table 3
Percent cover and ASTER estimated ET (mm day^{-1}) for the area of Entrada MODIS pixels 1 through 8.

MODIS pixel	Saltcedar % area	Willow/other veg. % area	Soil % area	Water % area	2005 est. ET	2006 est. ET	2007 est. ET
1	47.4	6.9	30.2	15.5	4.09	4.16	3.32
2	64.7	0	29.3	6.0	4.22	4.20	2.84
3	28.7	10.2	43.7	17.4	3.40	3.30	2.69
4	18.0	0	76.0	6.0	2.73	2.70	2.54
5	51.5	6.9	27.9	13.7	2.50	1.97	1.69
6	22.7	0	77.3	0	4.66	5.17	3.74
7	46.5	5.3	35.6	12.6	4.76	5.13	4.20
8	40.2	0	59.8	0	3.22	2.19	2.31
Mean	39.96	3.66	47.48	8.90	3.70[a]	3.60[a]	2.92[b]
SEM	(5.59)	(1.46)	(7.35)	(2.42)	(0.30)	(0.40)	(0.29)

Percent cover was measured using a point intercept classification of the NAIP data. ET means followed by different letters were significantly different at $P<0.01$ by Student's Paired *t*-Test. Standard Error of Mean values are shown in parentheses.

Table 4
Mean daily and annual ET estimated by MODIS EVI for the eight MODIS pixels comprising the Entrada site.

Year	Mean Daily ET DOY 73–313 mm/day	Annual ET DOY 73–313 m/year
2000	2.94 (0.28)	0.707 (0.068)
2001	2.69 (0.30)	0.648 (0.073)
2002	2.28 (0.25)	0.549 (0.059)
2003	2.51 (0.33)	0.602 (0.081)
2004	2.82 (0.29)	0.677 (0.086)
2005	2.55 (0.29)	0.614 (0.071)
2006	2.69 (0.35)	0.647 (0.085)
2007	2.86 (0.38)	0.686 (0.092)
Mean — all years	2.67 (0.08)	0.641 (0.014)

Standard Error of Mean values are shown in parentheses.

The NAIP point intercept classification of land cover showed that tamarisk accounted for approximately 40% of the area within the eight Entrada MODIS pixels, with a Standard Error of Mean (SEM) = 5.6% (Table 3). Other vegetation, including willows and emergent species, averaged only 4% of the area (SEM = 1.5%) within the eight MODIS pixels, but exceeded 10% cover in one pixel. Bare soil and water accounted for over 50% of the land cover within the riparian corridor. ET values estimated from the ASTER data were similar in 2005 and 2006, but decreased significantly ($P<0.01$) in 2007 following defoliation. ET estimated from the 2007 ASTER data was approximately 20% lower than ET estimated from the 2005 and 2006 ASTER data and the decrease was significant at $P<0.01$ (Table 3). However, this decrease in estimated ET was smaller than the 57% decrease in sap flux density between the mean pre-defoliation value and the value measured on the date of the 2007 ASTER acquisition.

The MODIS time series was used to examine longer term differences in estimated ET over the entire growing season. Mean daily ET and total annual ET estimated from MODIS data were not significantly different in 2007 compared to previous years (Table 4). Time series ET calculated from MODIS data showed considerable year-to-year variability even before *Diorhabda* was released. Overall, both ASTER and MODIS estimated ET values were moderate, amounting to less than half of potential evapotranspiration (e.g., approximately 2.0 m $year^{-1}$ on the Lower Colorado River Owen-Joyce & Raymond, 1996). Moderate estimated ET rates were caused by sparse vegetation cover. Less than half of the idealized MODIS pixel area was found to be densely vegetated by the point intercept classification (Table 3).

5. Discussion

Despite partial refoliation of tamarisk stands within the study area before ASTER data were acquired in 2007, threshold change in NDVI was able to detect defoliation that occurred within polygons dominated by tamarisk. It is often the case that higher spatial resolution remotely sensed data are infrequently acquired, but this limitation may not be a severe constraint on the use of ASTER and similar remotely sensed data. Spectral evidence of defoliation by *Diorhabda*, in the form of reduced NDVI, was still apparent more than 50 days after the start of the defoliation event (as measured by the sap flux data). The persistence of the defoliation signal in ASTER data still needs to be quantified to determine the length of the temporal window available to detect defoliation. The sap flux data

indicate that this signal may persist until the end of the growing season, in which case 1–2 ASTER acquisitions per year might be sufficient for mapping defoliated area.

False detections of defoliation are possible, especially when the locations of tamarisk stands are not known *a priori* and other land cover types are included in defoliation detection. Cultivated vegetation, such as alfalfa fields, produced the most obvious false detections in the defoliation map derived from ASTER data (Fig. 5). These false detections may be largely unavoidable, since crop type and phenology change from year to year. Pre-existing knowledge of farm locations would help avoid improper interpretation of NDVI trends. Disturbance may also lead to a false detection of defoliation by *Diorhabda*. Conventional tamarisk treatments, including herbicidal applications and mechanical clearing, may produce changes in NDVI similar to those seen for *Diorhabda* infestation. Disturbance of non-tamarisk vegetation may also result in false detection of defoliation. Spatial misregistration of multidate images is a major concern for false detection. Subpixel registration errors may result in changes in NDVI that exceed thresholds for detection. Errors produced by misregistration will be most obvious on the edges of vegetation stands where NDVI may rapidly decrease over short distances. The rate of false detection under different conditions should be explored by future research.

The primary concern for monitoring defoliation using MODIS data is the small percentage of each MODIS pixel covered by tamarisk. Tamarisk-dominated polygons covered less than 30% of any MODIS pixel in the study area, and the point intercept classification of the pixels making up the Entrada site showed a maximum tamarisk coverage of 65% (Table 3). For both the polygons and the point intercept classification, the average tamarisk coverage was well below 50%. Despite limited subpixel coverage of tamarisk, defoliation was still apparent in the MODIS time series based on the timing of EVI decline. At four of the five sites, EVI decline (as measured by ΔEVI_{min}) occurred anomalously early in the growing season. EVI decline in response to defoliation varied by site (Fig. 6). Tamarisk percent cover may control the magnitude of the EVI decline, but correlations between MODIS pixel percent polygon cover and 2007 EVI decline were not significant. A thresholding approach for detecting defoliation in MODIS data would require a measure of EVI decline as a percentage of long-term EVI, and would be most sensitive for pixels with higher tamarisk cover.

The temporal resolution of the ΔEVI_{min} method may be insufficient for operational monitoring of tamarisk defoliation. The demonstrated method requires more than one month of MODIS data to detect the large drop in EVI caused by defoliation. Using shorter compositing periods or even daily data may improve temporal resolution, but at the expense of increased EVI time series variability caused by view zenith angle effects. Based on the tradeoffs between temporal resolution and time series variability, MODIS data may be best suited to monitoring defoliation events over large areas, weeks to months after they begin. MODIS data could potentially be used to monitor the entire Colorado River Basin for defoliation by *Diorhabda*, including relatively inaccessible reaches of the Colorado and Green Rivers inside Grand Canyon National Park and Canyonlands National Park, respectively.

A primary motivation of *Diorhabda* release is to achieve water salvage by reducing tamarisk ET in riparian corridors. While this study documents a measureable decrease in ET in response to defoliation of tamarisk by *Diorhabda*, annual ET estimated by MODIS was not significantly different from previous years. Thus, the potential amount of water salvage due to defoliation remains difficult to determine. The 2007 defoliation event occurred following the spring and early summer green-up period, limiting reduced ET to the latter half of the growing season. Also, defoliated branches began to regenerate new leaves after about 20 days, resulting in a partial recovery of ET. If defoliation were to occur earlier in the next growing season or if repeated defoliation were to occur, potential water savings might increase. It is also not known whether any replacement vegetation could achieve ET rates as high as or higher that those observed in tamarisk stands.

Sap flux density measurements demonstrated a sharp decrease in transpiration at an early date. The histograms of ASTER NDVI before and after defoliation show similarly dramatic changes in the distribution of NDVI values, although the timing of these changes can not be determined from the ASTER data. MODIS ET estimates demonstrated a more subtle decline in ET following defoliation, and this decline lagged the decline in sap flux density. The MODIS pixels included other types of vegetation besides tamarisk, as well as bare soil and open water. As a result of coarse spatial and temporal sampling, MODIS EVI values may not have captured the transient ET response shown in the sap flux data. Further study, including field measurement of leaf area index, is needed to reconcile the timing of the declines in sap flux density and EVI. It is possible the beetles induce a stress reaction in plants that leads to an immediate reduction in stomatal conductance, captured by sap flux measurements, followed later by a drop in foliage densities as the plants are defoliated, captured by EVI.

This evaluation of the suitability of ASTER and MODIS data for monitoring tamarisk defoliation by *Diorhabda* was based on examination of trends in areas known to be dominated by tamarisk (e.g. the field-validated polygons). Remote monitoring of tamarisk defoliation is likely to be most successful in riparian areas where tamarisk is the dominant perennial species. In areas where tamarisk is sub-dominant and cover is sparse, defoliation detection and monitoring using remotely sensed data will be much more difficult.

6. Conclusions

Both ASTER and MODIS data have utility for remote monitoring of the occurrence, extent, and timing of tamarisk defoliation by the saltcedar leaf beetle. Although our study area is small relative to the extent of tamarisk invasion across the Western U.S. and to the monitoring abilities of MODIS, the results from this study should be applicable to larger areas as *Diorhabda* spreads. Our results highlight the importance of temporal resolution, spatial resolution, and spatial coregistration for detecting the occurrence of defoliation. Changes in NDVI calculated from multidate ASTER data can detect defoliation even after partial refoliation has occurred. MODIS data are capable of monitoring defoliation over larger areas, which is important given the limited accessibility of riparian corridors on the Colorado Plateau. Although tamarisk stands had limited fractional coverage at the minimum spatial resolution of MODIS data, defoliation was still evident as an abnormally early decline in EVI. Decreased ET associated with defoliation was predicted using both ASTER and MODIS data. However, the inter-annual variability in MODIS estimated annual ET values were as large as the change in annual ET caused by the initial defoliation event which happened towards the middle of the growing season. Insufficient ASTER and MODIS estimated ET data are available at present to predict whether or not tamarisk defoliation is likely to affect long-term water salvage.

Now that *Diorhabda elongata* is becoming established across eastern Utah, tamarisk defoliation is expected to occur annually in the future. The responses of tamarisk to these repeated defoliation events and the impacts of repeated defoliation on ecosystem processes are largely unknown. The remote sensing methodology demonstrated in this paper is likely to be an important tool for monitoring future defoliation events and their impacts on ecosystem processes. This study also provides an example of how remote sensing can be used to better understand, in a quantitative manner, the effectiveness of invasive species mitigation activities.

Acknowledgements

The authors would like to thank the University of Oregon, Solar Radiation Monitoring Lab Director, Frank Vignola (http://solardat.uoregon.edu/) for providing assistance with the Moab temperature data.

References

Allen, R., Tasumi, M., & Trezza, R. (2007). Satellite-based energy balance for mapping evapotranspiration with internalized calibration (METRIC) — model. *Journal of Irrigation and Drainage Engineering — ASCE*, *133*, 380—394.

Bailey, J., Schweitzer, J., & Whitham, T. (2001). Saltcedar negatively effects biodiversity of aquatic macroinvertebrates. *Wetlands*, *21*, 442—447.

Bastiaanssen, W., Menenti, M., Feddes, R., & Holtstaag, A. (1998). A remote sensing surface energy balance algorithm for land (SEBAL) — 1. Formulation. *Journal of Hydrology*, *213*, 198—212.

Busch, D. E., & Smith, S. D. (1995). Mechanisms associated with decline of woody species in riparian ecosystems of the southwestern U.S. *Ecological Monographs*, *65*, 347—370.

Carlson, T. (2007). An overview of the "triangle method" for estimating surface evapotranspiration and soil moisture from satellite imagery. *Sensors*, *7*, 1612—11629.

Cleugh, H., Leuning, R., Mu, Q., & Running, S. (2007). Regional evaporation estimates from flux tower and MODIS satellite data. *Remote Sensing of Environment*, *106*, 285—304.

Coops, N. C., Johnson, M., Wulder, M. A., & White, J. C. (2006). Assessment of QuickBird high spatial resolution imagery to detect red attack damage due to mountain pine beetle infestation. *Remote Sensing of Environment*, *103*, 67—80.

DeLoach, C. J., Carruthers, R. I., Lovich, J. E., Dudley, T. L., & Smith, S. D. (2000). Ecological interactions in the biological control of saltcedar (*Tamarix* spp.) in the United States: toward a new understanding. In N. R. Spencer (Ed.), *Proceedings of the X International Symposium on Biological Control of Weeds* (pp. 819—873). Bozeman, MT: Montana State University.

Dennison, P. E., Roberts, D. A., & Peterson, S. H. (2007). Spectral shape-based temporal compositing algorithms for MODIS surface reflectance data. *Remote Sensing of Environment*, *109*, 510—522.

DiTomosa, J. (1998). Impact, biology, and ecology of saltcedar (*Tamarix* spp.) in the southwestern United States. *Weed Technology*, *12*, 326—336.

Dudley, T. L. (2005). Progress and pitfalls in the biological control of saltcedar (*Tamarix* spp.) in North America. *Proceedings of the 16th U.S. Department of Agriculture Interagency Research Forum on Gypsy Moth and Other Invasive Species* GTR-NE-337.

Dudley, T. L., DeLoach, C. J., Lewis, P. A., & Carruthers, R. I. (2001). Cage tests and field studies indicate leaf-eating beetle may control saltcedar. *Ecological Restoration*, *19*, 260—261.

Franklin, S. E., Bowers, W. W., & Ghitter, G. (1995). Discrimination of adelgid-damage on single balsam fir trees with aerial remote sensing data. *International Journal of Remote Sensing*, *16*, 2779—2794.

Franklin, S. E., & Raske, A. G. (1994). Satellite remote sensing of spruce budworm forest defoliation in western Newfoundland. *Canadian Journal of Remote Sensing*, *20*, 37—48.

Franklin, S. E., Waring, R. H., McCreight, R. W., Cohen, W. B., & Fiorella, M. (1995). Aerial and satellite sensor detection and classification of western spruce budworm defoliation in a subalpine forest. *Canadian Journal of Remote Sensing*, *21*, 299—308.

Franklin, S. E., Wulder, M. A., Skakun, R. S., & Carroll, A. L. (2003). Mountain pine beetle red-attack forest damage classification using stratified Landsat TM data in British Columbia, Canada. *Photogrammetric Engineering and Remote Sensing*, *69*, 283—288.

Fraser, R. H., & Latifovic, R. (2005). Mapping insect-induced tree defoliation and mortality using coarse spatial resolution satellite imagery. *International Journal of Remote Sensing*, *26*, 193—200.

Glenn, E. P., & Nagler, P. L. (2005). Comparative ecophysiology of *Tamarix ramosissima* and native trees in western U.S. *riparian zones. Journal of Arid Environments*, *61*, 419—446.

Granier, A. (1987). Evaluation of transpiration in a Douglas fir stand by means of sap flow measurements. *Tree Physiology*, *3*, 309—320.

Granier, A. (1996). *Sap Flow Measurements Using the Radial Flowmeter Technique* (pp. 1—9). Champenoux: INRA-Unité d'Ecophysiologie Forestiére.

Holben, B. N. (1986). Characteristics of maximum value composite images from temporal AVHRR data. *International Journal of Remote Sensing*, *7*, 1417—1434.

Holben, B. N., & Fraser, R. S. (1984). Red and near-infrared sensor response to off-nadir viewing. *International Journal of Remote Sensing*, *5*, 145—160.

Huete, A. R., Didan, K., Miura, T., Rodriguez, E. P., Gao, X., & Fereira, L. G. (2002). Overview of the radiometric and biophysical performance of the MODIS vegetation indices. *Remote Sensing of Environment*, *83*, 195—213.

Hultine, K. R., Bush, S. E., West, A. G., & Ehleringer, J. R. (2007). The effect of gender on sap-flux scaled transpiration in a dominant riparian tree species: box elder (*Acer negundo*). *Journal of Geophyscal Research*, *112*, G03S06.

Leckie, D. G., & Ostaff, D. P. (1988). Classification of airborne multispectral scanner data for mapping current defoliation caused by the spruce budworm. *Forest Science*, *34*, 259—275.

Johnson, S. (1987). Can saltcedar be controlled? *Fremontia*, *15*, 19—20.

Joria, P. E., Ahearn, S. C., & Connor, M. (1991). A comparison of the SPOT and Landsat Thematic Mapper satellite systems for detection gypsy moth defoliation in Michigan. *Photogrammetric Engineering and Remote Sensing*, *57*, 1605—1612.

Kustas, W., & Norman, J. (1999). Evaluation of soil and vegetation heat flux predictions using a simple two-source model with radiometric temperatures for partial canopy cover. *Agricultural and Forest Meteorology*, *94*, 13—29.

Mann, H. B., & Whitney, D. R. (1947). On a test of whether one of two random variables is stochastically larger than the other. *Annals of Mathematical Statistics*, *18*, 50—60.

Mildrexler, D. J., Zhao, M., Heinsch, F. A., & Running, S. W. (2007). A new satellite-based methodology for continental-scale disturbance detection. *Ecological Applications*, *17*, 235—250.

Monteith, J. L., & Unsworth, M. H. (1990). *Principles of Environmental Physics*, Second ed. London: Edward Arnold.

Mu, Q., Heinsch, F., Zhao, M., & Running, S. (2007). Development of a global evapotranspiration algorithm based on MODIS and global meteorology data. *Remote Sensing of Environment*, *111*, 519—536.

Nagler, P., Cleverly, J., Lampkin, D., Glenn, E., Huete, A., & Wan, Z. (2005). Predicting riparian evapotranspiration from MODIS vegetation indices and meteorological data. *Remote Sensing of Environment*, *94*, 17—30.

Nagler, P., Glenn, E., Hursh, K., Curtis, C., & Huete, A. (2005). Vegetation mapping for change detection on an arid-zone river. *Environmental Monitoring and Assessment*, *109*, 255—274.

Nagler, P. L., Glenn, E. P., Kim, H., Emmerich, W. E., Scott, R. L., & Huxman, T. E. (2007). Seasonal and interannual variation of evapotranspiration for a semiarid watershed estimated by moisture flux towers and MODIS vegetation indices. *Journal of Arid Environments*, *70*, 443—462.

Nagler, P., Jetton, A., Fleming, J., Didan, K., Glenn, E., & Morino, K. (2007). Evapotranspiration in a cottonwood (*Populus fremontii*) restoration plantation estimated by sap flow and remote sensing methods. *Agricultural and Forest Meteorology*, *144*, 95—110.

Nagler, P., Scott, R., Westenburg, C., Cleverly, J., Glenn, E., & Huete, A. (2005). Evapotranspiration on western U.S. rivers estimated by the Enhanced Vegetation Index from MODIS and data from eddy covariance and Bowen ratio flux towers. *Remote Sensing of Environment*, *97*, 337—351.

Nelson, R. F. (1983). Detecting forest canopy change due to insect activity using Landsat MSS. *Photogrammetric Engineering and Remote Sensing*, *49*, 1303—1314.

Owen-Joyce, S. J., & Raymond, L. H. (1996). An accounting system for water and consumptive use along the Colorado River, Hoover Dam to Mexico. *U.S. Geological Survey Water-Supply Paper 2407* 94 pp.

Owens, M. K., & Moore, G. W. (2007). Saltcedar water use: realistic and unrealistic expectations. *Rangeland Ecology and Management*, *60*, 553—557.

Penny, R. (1991). *The Whitewater Sourcebook: A Directory of Information on American Whitewater Rivers.* Birmingham, AL: Menasha Ridge Press.

Qi, J., & Kerr, Y. (1997). On current compositing algorithms. *Remote Sensing Reviews*, *15*, 235—256.

Radeloff, V. C., Mladenoff, D. J., & Boyce, M. S. (1999). Detecting jack pine budworm defoliation using spectral mixture analysis: separating effects from determinants. *Remote Sensing of Environment*, *69*, 156—169.

Renz, A. N., & Nemeth, J. (1985). Detection of mountain pine beetle infestation using Landsat MSS and simulated Thematic Mapper data. *Canadian Journal of Remote Sensing*, *13*, 92—95.

Rice, J., Anderson, B., & Ohmert, R. (1980). Seasonal habitat selection by birds in the Lower Colorado River Valley. *Ecology*, *61*, 1402—1411.

Rohnde, W. G., & Moore, H. J. (1974). Forest defoliation assessment with satellite imagery. *Proceedings of the 9th International Symposium on Remote Sensing of the Environment* (pp. 1089—1104). Ann Arbor: University of Michigan.

Rouse, J. W., Haas, R. H., Schell, J. A., & Deering, D. W. (1973). Monitoring vegetation systems in the Great Plains with ERTS. *Third ERTS Symposium, NASA: SP351*, *1*, 309—317.

Royle, D. D., & Lathrop, R. G. (2002). Discriminating *Tsuga canadensis* hemlock forest defoliation using remotely sensed change detection. *Journal of Nematology*, *34*, 213—221.

Scott, R. L., Cable, W. L., Huxman, T. E., Nagler, P. L., & Goodrich, D. C. (2008). Multiyear riparian evapotranspiration and groundwater use for a semiarid watershed. *Journal of Arid Environments* published online.

Sirois, J., & Ahern, F. J. (1988). An investigation of SPOT HRV data for detecting mountain pine beetle mortality. *Canadian Journal of Remote Sensing*, *14*, 104—108.

Smith, S., Devitt, D., Sala, A., Cleverly, J., & Busch, D. (1998). Water relations of riparian plants from warm desert regions. *Wetlands*, *18*, 687—696.

Stromberg, J. (1998). Functional equivalency of saltcedar (*Tamarix chinensis*) and Fremont cottonwood (*Populus fremontii*) along a free flowing river. *Wetlands*, *18*, 675—686.

Townsend, P. A., Eshleman, K. N., & Welcker, C. (2004). Remote sensing of gypsy moth defoliation to assess variations in stream nitrogen concentrations. *Ecological Applications*, *14*, 504—516.

White, J. C., Coops, N. C., Hilker, T., Wulder, M. A., & Carroll, A. L. (2007). Detecting mountain pine beetle red attack damage with EO-1 Hyperion moisture indices. *International Journal of Remote Sensing*, *28*, 2111—2121.

Wolfe, R. E., Roy, D. P., & Vermote, E. F. (1998). The MODIS land data storage, gridding and compositing methodology: level 2 grid. *IEEE Transactions Geoscience and Remote Sensing*, *36*, 1324—1338.

Wulder, M. A., Dymond, C. C., White, J. C., Leckie, D. G., & Carroll, A. L. (2005). Surveying mountain pine beetle damage of forests: a review of remote sensing opportunities. *Forest Ecology and Management*, *221*, 27—41.

Yang, F., White, A., Michaelis, A., Ichii, K., Hashimoto, H., & Votava, P. (2006). Prediction of continental-scale evapotranspiration by combining MODIS and AmeriFlux data through support vector machine. *IEEE Transactions on Geoscience and Remote Sensing*, *44*, 3452—3461.

Zavaleta, E. (2000). The economic value of controlling an invasive shrub. *Ambio*, *29*, 462—467.